ELSEVIER

Contents lists available at ScienceDirect

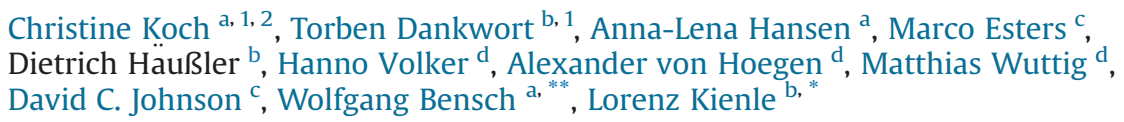
## Acta Materialia

journal homepage: www.elsevier.com/locate/actamat



## Full length article

## Investigation of the phase change mechanism of Ge<sub>6</sub>Sn<sub>2</sub>Sb<sub>2</sub>Te<sub>11</sub>





<sup>&</sup>lt;sup>b</sup> Institute for Materials Science, Kiel University, Kaiserstrasse 2, 24143, Kiel, Germany



#### ARTICLE INFO

Article history: Received 14 February 2018 Received in revised form 11 April 2018 Accepted 12 April 2018 Available online 17 April 2018

Keywords:
Phase change material (PCM)
In situ transmission electron microscopy
(TFM)

#### ABSTRACT

Thin films of  $Ge_6Sn_2Sb_2Te_{11}$  were synthesized and compared to the well-known unsubstituted phase change material (PCM)  $Ge_8Sb_2Te_{11}$ . In situ X-ray diffraction (XRD) and temperature dependent sheet resistance measurements evidenced a significant decrease of the phase change temperature from  $144^{\circ}C$  for  $Ge_8Sb_2Te_{11}$  to  $112^{\circ}C$  for  $Ge_6Sn_2Sb_2Te_{11}$ . The resistance measurements also revealed an intermediate step during the phase change. Detailed in situ transmission electron microscopy (TEM) and (XRD) investigations on structural ordering phenomena suggest that this intermediate step is associated with the disorder of structural vacancies on the cationic sites stable up to  $130^{\circ}C$ . Annealing the sample beyond  $130^{\circ}C$  leads to a subsequent ordering of vacancies and thus to the formation of a metastable primitive trigonal phase with vacancy layers. At  $\sim 240^{\circ}C - \sim 300^{\circ}C$ , a transition to the stable phase is observed. For the first time, an in plane movement of bi-layer defects is observed by in situ TEM as a result of a self-ordering mechanism. These findings represent new insights into the transition process on the nanoscale and suggest that tin substituted PCMs may represent promising candidates for multi-level data storage applications.

© 2018 Acta Materialia Inc. Published by Elsevier Ltd. All rights reserved.

## 1. Introduction

In 1968, S. R. Ovshinsky described a "rapid and reversible transition between a highly resistive and a conductive state" in amorphous semiconductors [1]. After the identification of GeTe as a promising candidate for optical data storage in 1986, studies focused on materials on the pseudobinary section of GeTe and Sb<sub>2</sub>Te<sub>3</sub> (GST-materials), showing good optical contrast between the high reflecting crystalline and the less reflecting amorphous phase as well as fast recrystallization speed [2–9]. As a result, Ge-Sb-Te based alloys are used as the active material in optical data storage devices such as compact discs (CD) and digital versatile disc (DVD) materials as well as Blu-ray<sup>TM</sup> discs [10].

These materials are characterized by two metastable phases, usually an amorphous and a crystalline one, with significantly different optical and electrical properties. While the short-range order of the atoms in the amorphous phase is still intensely discussed in literature [11,12], the metastable crystalline phase crystallizes in a distorted rock-salt structure with varying concentrations of randomly distributed vacancies on the cation sites (so called structural vacancies), depending on the chemical composition [8,13e18]. At elevated temperatures, these vacancies start to order along the (111)<sub>c</sub> planes (subscript c denotes the cubic NaCl-aristotype structure). Depending on the degree of ordering, the formation of different phases is reported. The observed phases can all be treated as a three dimensionally twinned version of a trigonal phase with a rock salt stacking sequence with respect to the Te sublattice [19,20].

PCMs can also be rapidly and reversibly switched from the conductive crystalline phase to the insulating amorphous phase. Short and intense electrical pulses are used to switch from the crystalline phase to the amorphous state (reset pulse), while for recrystallization, a longer electrical pulse (set pulse) is used. Due to the fast switching speeds and the resulting electrical contrast of ~3

<sup>&</sup>lt;sup>c</sup> Department of Chemistry and Material Science Institute, University of Oregon, Eugene, OR, 97403, United States

d Institute of Physics, RWTH Aachen University, Sommerfeldstrasse 14, 52056, Aachen, Germany

<sup>\*</sup> Corresponding author.

<sup>\*\*</sup> Corresponding author.

E-mail addresses: wbensch@ac.uni-kiel.de (W. Bensch), lk@tf.uni-kiel.de

<sup>&</sup>lt;sup>1</sup> Authors contributed equally.

 $<sup>^2\,</sup>$  Present address: University of Applied Sciences Bremerhaven, An der Karlstadt 8, 27568 Bremerhaven.

orders of magnitude between the two states, these materials can serve as data storage materials in nonvolatile electronic memory devices (PCRAM). Furthermore, some PCMs show a more gradual transition from the insulating to the conductive state. Consequently, materials with two or three metastable intermediate resistance levels are promising candidates for multi-level data storage devices [10,21e24].

Especially well investigated are the amorphous and the crystalline phases of GeTe [25], Ge 2Sb2Te5 [26-35] and Ge8Sb2Te11 [6,9,36]. Since these materials have already reached the limits for application in current data storage devices, many new compounds are being investigated, e.g. Ga-Sb alloys [37–39], GeCu <sub>2</sub>Te<sub>3</sub> [40–42] and AIST [28,33,43] (AIST =  $\mathbf{Ag}$ , In,  $\mathbf{Sb}$  and  $\mathbf{Te}$ ). Many studies have also investigated the doping or the substitution of well investigated materials to improve properties, such as Ge-doped Sb [44], Ge 15Sb<sub>85</sub> [45] and GaSb [46]. Substitution and doping of Ge 2Sb<sub>2</sub>Te<sub>5</sub> and Ge<sub>8</sub>Sb<sub>2</sub>Te<sub>11</sub> have also been extensively explored, with reports of N- [47,48], C- [49], In- [50], Se- [51] and Bi- [52] substituted Ge<sub>2</sub>Sb<sub>2</sub>Te<sub>5</sub>, Se- and Sn-doped [52-54] Ge<sub>2</sub>Sb<sub>2</sub>Te<sub>5</sub>, and Bi- [55], Sn-[56] and Se- [56] substituted Ge <sub>8</sub>Sb<sub>2</sub>Te<sub>11</sub> [57]. These studies revealed interesting variations of phase change characteristics, such as enhanced optical and electrical properties or higher stability. Additionally, novel features such as thermoelectric properties of GeTe-rich GST [58,59] and Se- [60] substituted or CoGe 2-doped GST-materials [61] have been reported. However, the structures of the doped or substituted compounds, and the relation between doping/substitution level, crystal structure and resulting properties are not well understood. Understanding the influence of single element substitution on the structure and properties of GST-based materials is crucial for the development of new PCMs.

One of the most promising candidates for future applications are Sn substituted GST-materials. It was already reported that tin substitution of Ge <sub>2</sub>Sb<sub>2</sub>Te<sub>5</sub> leads to a decrease in the phase change temperature and to a significant increase in the optical contrast (up to 40% compared to 15% for pure Ge <sub>2</sub>Sb<sub>2</sub>Te<sub>5</sub> [62]), which is an excellent feature for optical phase change memory applications. Furthermore, ultra-fast crystallization speed and a reduced activation energy were described, as well as enhanced thermoelectric properties for the corresponding bulk materials [60,62–64]. Despite these improvements of the properties, the actual phase change mechanism and the electrical properties were not investigated in detail so that no structure property relations could be established.

Because of the excellent combination of properties of tin substituted GST, we decided to prepare Sn substituted Ge 8Sb2Te11 (Ge 6Sn<sub>2</sub>Sb<sub>2</sub>Te<sub>11</sub>) and focus our investigations on the phase change process and the occurrence of metastable crystalline phase(s). During our experiments, we discovered through a combined approach of in situ TEM and XRD investigations that the metastable regime consists of varying phase mixtures. At 117 °C-130 °C, a mixture of cubic and rhombohedral (a distorted rock salt) structure was observed, which appeared as a (pseudo) cubic phase with vacancies disordered on the cationic sites (structural vacancies). At 130 °C, an additional primitive trigonal phase with vacancies ordered inside the (111)<sub>c</sub> planes forming vacancy layers was observed using in situ TEM. For the latter phase, a subsequent increase in ordering of the vacancies was observed upon heating. In the temperature range of 240 °C–300 °C, the transition to the stable phase was observed. For the stable phase, an in-plane movement of bilayer defects was directly observed and highlights the selfordering process of the vacancies in the stable phase. The metastable phases and the stable phase can be clearly separated by their

stacking sequence to a hexagonal type stacking across the Te-Te layers, and a van der Waals gap is formed [19,20]. In accordance with our TEM and XRD investigations, temperature dependent sheet resistance measurements revealed a unique intermediate resistance step during annealing that may be used in electrical multi-level data storage media.

#### 2. Experimental procedures

Ge $_8$ Sb $_2$ Te $_{11}$  samples were prepared by DC magnetron sputtering using stoichiometric targets (umicore, 99.99%, 10 cm Ø) bonded to water cooled copper plates. The argon flow was fixed at 20 sccm during the depositions. To ensure stable deposition rates, the base pressure in the sputter chamber ( $<2 \cdot 10^{-6}$  mbar), applied power and temperature were monitored during the deposition process. For TEM measurements, thin films of ~30 nm thickness were prepared in 276 s on nickel TEM-grids and coated with a thin amorphous carbon layer. Samples of ~630 nm thickness were deposited in 7735 s on different substrates, e.g. (100) silicon single crystals (with a size of 2 cm  $\times$  2 cm) and glass substrates with and without sputtered chromium contacts (~200 nm thickness) for the electrical measurements. The sizes of the samples for the electrical sheet resistance measurements were 1 cm  $\times$  1 cm.

Thin film samples of  $Ge_6Sn_2Sb_2Te_{11}$  were synthesized by coevaporation of the elements in a high vacuum chamber at pressures  $<2\times10^{-6}$  mbar. Ge and Sn were deposited using electron beam guns while Sb and Te were evaporated by effusion cells. The resulting deposition rates were monitored by quartz crystal microbalances and are listed in Table S1 in the supplementary material. Thin films of ~35 nm thickness and thicker samples of 500-600 nm thickness were prepared in 450 s and 6750 s, respectively, using the same substrates as for the unsubstituted materials.

A Cameca SX 100 electron probe microanalysis system (EPMA) was used to determine the sample compositions by investigating the L lines of the elements with acceleration voltages of 10, 16 and 22 kV. Film thicknesses were obtained with a Bruker DektakXT profilometer.

For X-Ray diffraction (XRD), an X'Pert Pro MPD diffractometer (PANalytical, Cu  $K_\alpha$  radiation) equipped with a G obel mirror and a PIXcel detector was used. The measurements were carried out in  $\theta$ - $\theta$  geometry. In situ XRD measurements were performed with an Anton Paar HTK 1200 N high temperature chamber with helium (99.999%) atmosphere to prevent oxidation of the samples. The temperature was increased stepwise with a heating rate of 5 °C/min from 28 °C to 360 °C in steps of 5 °C (or 1 °C in the temperature region of the phase transition). Each pattern was collected within 1 h at constant temperature covering a 2  $\theta$  range of 15–65°.

For the structural refinements, samples of Ge  $_6\mathrm{Sn_2Sb_2Te_{11}}$  were annealed in helium atmosphere for 3 h in the Anton Paar HTK 1200 N high temperature chamber at 117 °C, 160 °C and 320 °C, respectively. The scans for the refinements were carried out on a flat stage (z-tilt-phi) in a range of 15–110 ° 2 $\theta$  with a step size of 0.03°. Pawley refinements were applied using Topas Academic Version 6 [65]. For the determination of the coherently scattering domains in the samples, the contribution of the instrument was modeled using the fundamental parameter approach [66].

For temperature dependent nanostructure investigations, a transmission electron microscope Tecnai F30 STwin was used. *In situ* heating experiments were performed in a Gatan 652 tantalum furnace double tilt heating holder. The heating rate was set to 5 °C/min. For image processing, Digital Micrograph and scripts [67] were

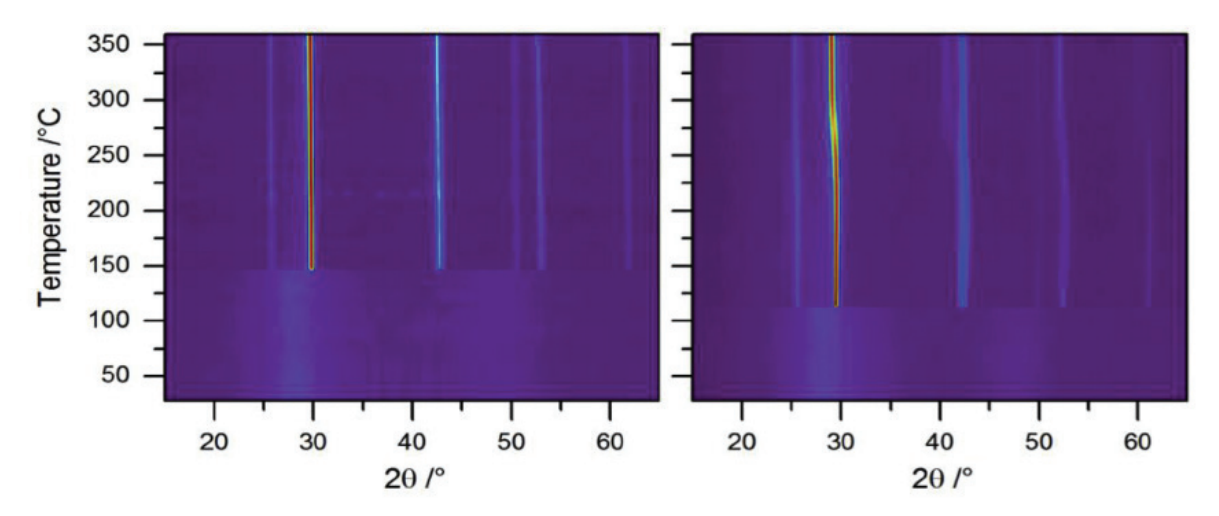
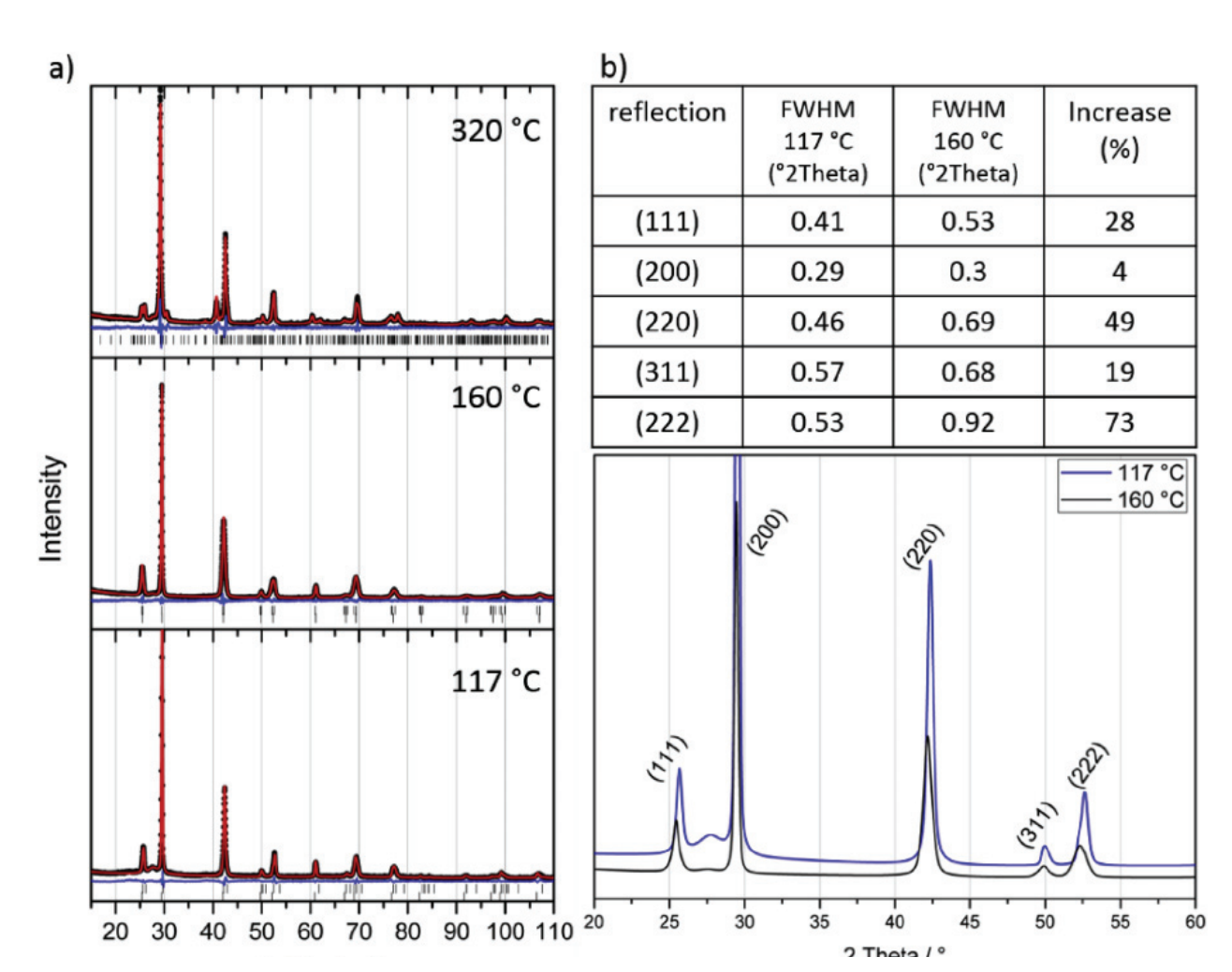


Fig. 1. In situ XRD patterns of Ge <sub>8</sub>Sb<sub>2</sub>Te<sub>11</sub> (left) and Ge <sub>6</sub>Sn<sub>2</sub>Sb<sub>2</sub>Te<sub>11</sub> (right). Phase changes can be seen by the appearance and disappearance of reflections.

Pauw [69,70] with argon (99.996%) as protective gas. The samples were heated up to 360  $^{\circ}$ C with a heating rate of 5  $^{\circ}$ C/min. This temperature was held constant for 30 min before the samples were cooled down to room temperature. Since the influence of the

thickness and density contrast upon the phase change could not be determined and corrected with this setup, the sheet-resistance is reported instead of the resistivity.



**Fig. 2.** a): Powder diffraction patterns of Ge  $_6$ Sn $_2$ Sb $_2$ Te $_{11}$  heated for 3 h at 117 °C, 160 °C and 320 °C (thermodynamically stable phase). Black circles depict the measured data, red lines the refined patterns and the blue lines display the difference between them. Reflection positions are marked by vertical bars. b) Top: full width at half maximum (FWHM) of reflections in the enlarged section below (20–60 ° 2 Theta region). The anisotropic broadening of the (hhh) and (hh0) reflections is clearly visible. The broad intensity at ~27.5 ° stems from a residual amorphous background.

C. Koch et al. / Acta Materialia 152 (2018) 278-287

**Table 1**Pawley refinement data from room temperature XRD-measurements of Ge <sub>8</sub>Sb<sub>2</sub>Te <sub>11</sub> from Ref. [9] and Ge<sub>6</sub>Sn<sub>2</sub>Sb<sub>2</sub>Te<sub>11</sub> (annealed at 117 ° C, 160 °C and 320 °C). Estimated standard deviations are given in parentheses.

Chemical Formula		Ge <sub>8</sub> Sb <sub>2</sub> Te <sub>11</sub> [9]		Ge <sub>6</sub> Sn <sub>2</sub> Sb <sub>2</sub> Te <sub>11</sub> at 117 °C		Ge <sub>6</sub> Sn <sub>2</sub> Sb <sub>2</sub> Te <sub>11</sub> at 160 °C		Ge <sub>6</sub> Sn <sub>2</sub> Sb <sub>2</sub> Te <sub>11</sub> at 320 °C
Space Group		R3m (160)	Fm3m (225)	R3m (160)	Fm3m (225)	R3m (160)	Fm3m (225)	P3m1 (164)
Cell Parameters (Å)	a c	4.2099(6) 10.247(4)	5.950(3) -	4.284(1) 10.229(5)	6.082(1) -	4.303(9) 10.44(6)	6.060(1) _	4.340(4) 42.06(5)
Crystallite size (nm) deviation from cubic symmetry		-	_	17(1) 2%	32(1)	11(1) 0.7%	33(1)	21(1)
$R_{\rm wp}$		8.5		6.7		6.7		8.6

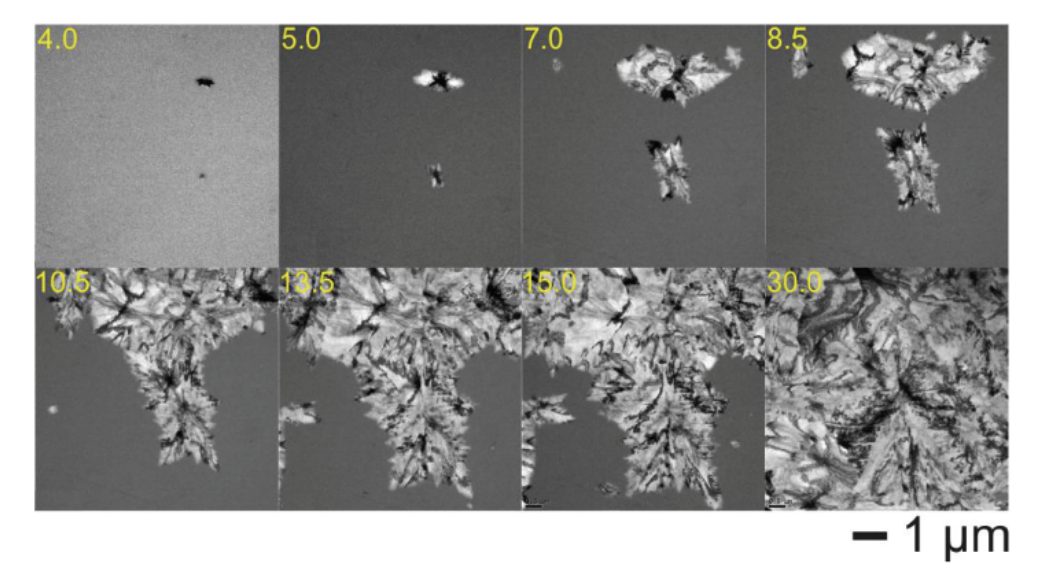


**Fig. 3.** TEM bright field images for an isothermal crystallization process at 125 °C for Ge<sub>6</sub>Sn<sub>2</sub>Sb<sub>2</sub>Te<sub>11</sub>. The yellow numbers mark the heating time in minutes. After 4 min, two crystallites have formed which rapidly grow. The sample is fully crystalline after ~30 min. (For interpretation of the references to colour in this figure legend, the reader is referred to the Web version of this article.)

#### 3. Results and discussion

# 3.1. Structural characterization by in situ XRD and in situ TEM measurements

In situ XRD was used to investigate the crystallization behavior and the influence of Sn on the phase change temperatures (Fig. 1). The studies revealed that the as deposited films of Ge  $_8$ Sb $_2$ Te $_{11}$  and Ge $_6$ Sn $_2$ Sb $_2$ Te $_{11}$  were in the amorphous state. For Ge $_8$ Sb $_2$ Te $_{11}$ , seemingly only one crystalline phase was observed during in situ heating experiments as the metastable and thermodynamically stable crystalline phases can hardly be distinguished due to their structural similarity. The first phase change temperature associated with the phase transition from the amorphous to a crystalline phase decreases significantly from 144 °C (Ge $_8$ Sb $_2$ Te $_{11}$ ) to 112 °C (Ge $_6$ Sn $_2$ Sb $_2$ Te $_{11}$ ) which is consistent with data reported in literature for Sn substituted Ge $_2$ Sb $_2$ Te $_{5}$ [63] and lower than previously reported for Ge $_8$ Sb $_2$ Te $_{11}$  [57]. Pawley refinement was used on the metastable phase of Ge $_6$ Sn $_2$ Sb $_2$ Te $_{11}$  annealed at two different

deviation from the cubic symmetry. For the sample heated to 160 °C, an anisotropic broadening of the reflections, particularly the (hhh) and (hh0) reflections (see Fig. 2 b), and a decreased deviation from the cubic symmetry (~0.7% compared to ~2% for the sample heated at 117 °C) is observed. Both observations indicate that the structural distortion at 117 °C is more of random nature, while it gets localized at 160 °C, indicated by a less distorted structure, but broadened (hhh) and (hh0) reflections. The phase change from the metastable phase to the thermodynamically stable state appears to be continuous over a relatively large temperature region (~240-~300 °C). For both the Ge<sub>8</sub>Sb<sub>2</sub>Te<sub>11</sub> and Ge<sub>6</sub>Sn<sub>2</sub>Sb<sub>2</sub>Te<sub>11</sub> samples, no decomposition or additional structural transitions were observed up to 360 °C (Fig. 1). Compared to the values reported for Ge<sub>8</sub>Sb<sub>2</sub>Te<sub>11</sub>, the metastable phases of the Sn-substituted samples exhibit a slight increase in the lattice parameters [9], which can be explained by the larger radius of Sn compared to Ge. The coherently scattering domain sizes of the cubic and rhombohedral phases are 32 nm and 17 nm for samples heated to 117  $\,^{\circ}$ C, 33 nm and 11 nm for the samples heated to 160 °C, and 21 nm for samples heated to

281

temperatures (117  $^{\circ}$ C and 160  $^{\circ}$ C, 3,h) and on the thermodynamically stable phase annealed at 320  $^{\circ}$ C (Fig. 2 and Table 1) to determine structural differences between the phases. Structural analysis of the XRD patterns at 117  $^{\circ}$ C and 160  $^{\circ}$ C revealed the existence of a mixture of a cubic ( $Fm\bar{3}m$ ) and a trigonal (R3m) phase, rather than a single one [9,57]. The trigonal phase can be described as a slightly distorted rock salt structure. Because of the structural similarity of both phases, we hypothesize that instead of two separate phases, the sample consists of small domains with varying degrees of

320°C. In situ TEM heating experiments were conducted on as deposited films of Ge<sub>6</sub>Sn<sub>2</sub>Sb<sub>2</sub>Te<sub>11</sub> using a heating rate of 5°C/min. To determine the phase change temperatures, the samples were monitored during the heating process by electron diffraction (ED) and high-resolution transmission electron microscopy (HRTEM). The temperature was kept constant during the ED and HRTEM measurements. ED patterns and HRTEM micrographs were taken from varying positions to minimize electron beam induced changes

C. Koch et al. / Acta Materialia 152 (2018) 278-287

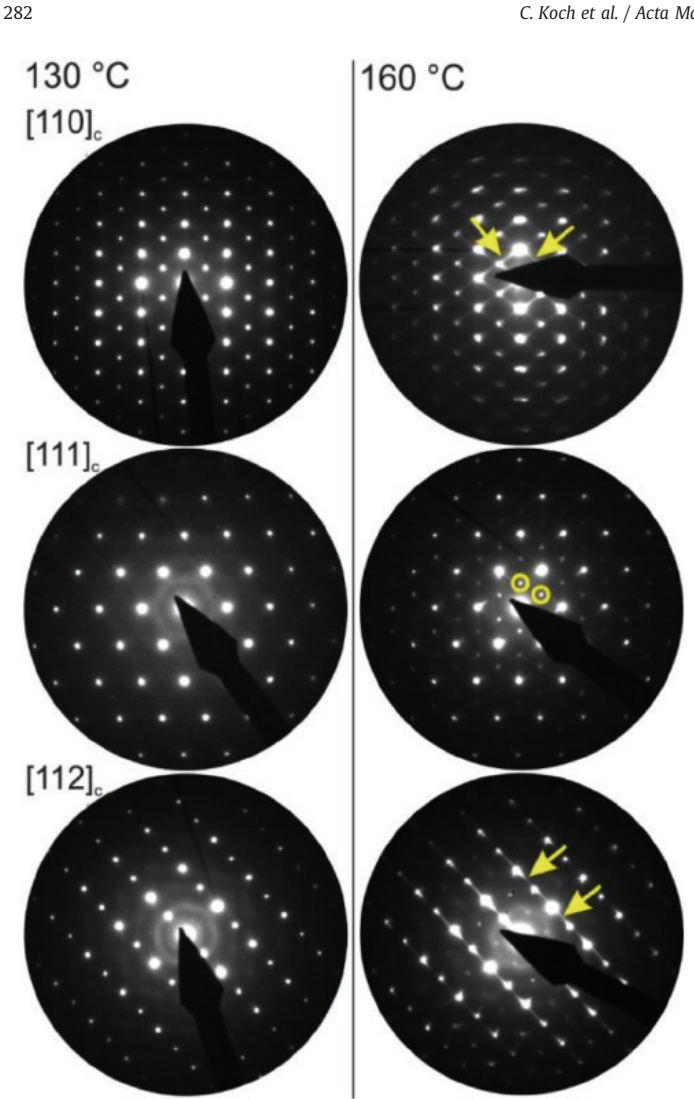


**Fig. 4.** Electron diffraction patterns recorded at 130  $^{\circ}$ C (left) and 160  $^{\circ}$ C (right) for different zone axes. Comparing both columns, a phase change is visible and can be attributed to ordering of vacancies along the (111) planes. Due to this ordering, superlattice reflections and diffuse intensities are observed (highlighted in yellow). (For interpretation of the references to colour in this figure legend, the reader is referred to the Web version of this article.)

[34]. The as deposited Ge <sub>6</sub>Sn<sub>2</sub>Sb<sub>2</sub>Te<sub>11</sub> films were completely amorphous. Grain growth and nucleation started at ~121 °C, which is consistent with the findings from *in situ* XRD. Fig. 3 shows a series of bright field images of Ge <sub>6</sub>Sn<sub>2</sub>Sb<sub>2</sub>Te<sub>11</sub> films taken during isothermally heating at 125 °C, and shows the growth process of the crystallites. After 30 min at 125 °C, the sample was completely crystalline. The nucleation rate appears to be relatively low compared to observations on other PCMs [51], indicating that the

Pawley refinements where the presence of a cubic and a rhombohedral or pseudo cubic phase was observed, as small deviations from the cubic symmetry were not resolvable by TEM. In the following text, we will refer to this presumed phase mixture as I. The absence of diffuse scattering in the zone axis [110] c indicates that structural vacancies are all randomly distributed on the cationic sites as observed for Ge 2Sb2Te5 [18,19]. Between 130 and 145 °C, structural vacancies start ordering in the (111) c planes forming vacancy layers. This leads to a phase transition from vacancy disordered I to a primitive trigonal phase II at 145 °C. Thus, in this intermediate temperature range, a phase mixture of I and II is present. The trigonal phase II can be identified by the presence of diffuse streaks along the <111> c directions and superstructure reflections that violate the fcc reflection conditions (yellow circles and arrows in Fig. 4). These findings explain the reflection broadening above 160 °C in the XRD patterns as this likely reflects the formation of (111)<sub>c</sub> vacancy layers. According to the reflection conditions, the observed superstructure reflections indicate trigonal P symmetry and exclude the formation of a trigonal R phase.

HRTEM micrographs recorded at 150 °C in zone axis [111]<sub>c</sub> (Fig. 5a)) depict the initial stage of the transition from I to the primitive trigonal phase II through ordering of the vacancies. This is evidenced by the formation of superlattice peaks in the Fourier transform (FFT) and suggests that a phase mixture of I and phase II is present. Fig. 5b) represents an inverse FFT filtered image based on the superstructure peaks (cf. Fig. 5d)). For inverse FFT filtering, regions with enhanced contrast appear if the superstructure peaks contribute to the HRTEM contrast. The inverse FFT filtering shows that the transition starts with the formation of coherent nanoscale domains that are 1–15 nm in size. The detailed view in Fig. 5c) depicts a ~15 nm large coherent domain with a characteristic honeycomb contrast due to the contributions of superlattice reflections. For Ge 2Sb2Te5, a similar phase is referred to as a vacancyordered cubic phase [19], emphasizing that the Te-layer stacking sequence is identical to the cubic disordered phase. Furthermore, extended electron beam irradiation of phase II leads to a disordering of the vacancies and consequently the diffuse scattering vanishes (Fig. S1 in the supplementary material). Due to the electron beam irradiation, the primitive trigonal phase II can be retransformed into disordered I, which is a common feature of GSTs [72] and other PCMs [73]. In recently observed cases, the samples can be selectively modified by an electron probe [74]. It can be speculated that the vacancy ordering phenomenon is a purely diffusion dominated process for the transition between the different phases, but in situ annealing for two hours at 150 °C of the metastable phase mixture of I and II did not yield a significant increase in ordering of the vacancies (see Fig. 6, left).

Increasing the temperature leads to increased ordering of the vacancies as observed by TEM micrographs and ED patterns shown in Fig. 6 (all along zone axis [110] <sub>c</sub>). For TEM micrographs, the linear arrays of bright and dark contrast stem from vacancy layers parallel

0

283

crystallization process for Ge $^6$ Sn $^2$ Sb $^2$ Te $^{11}$  is growth-driven and not nucleation-driven. A nucleation-driven process would also lead to the formation of nanocrystallites [33], but larger single crystalline areas with bending contours are observed for the Ge $^6$ Sn $^2$ Sb $^2$ Te $^{11}$ films. While the growth processes are similar to what was observed in other chalcogenides during  $in\ situ$  heating [34,71], there is strong anisotropic growth in the Ge $^6$ Sn $^2$ Sb $^2$ Te $^1$ films, which is a notable difference to what was observed for Ge $^2$ Sb $^2$ Te $^5$  [34].

Electron diffraction patterns and bright-field TEM images were recorded at elevated temperatures to monitor the phase changes (heating rate 5  $^{\circ}$ C/min). The first crystalline phase appearing upon heating (Fig. 4, left, recorded at 130  $^{\circ}$ C) exhibited a cubic or at least a pseudo cubic crystal structure. These results agree with XRD

to both {111}c planes, At 180 C, partial, unevenly distributed and intersecting vacancy layers are observed forming a parquet-like structure [58,75,76]. The degree of ordering increases with each temperature step and at 240 °C, few overlapping vacancy layers are observed, and domains with twin-like interfaces form. The vacancy layers are also more homogenously distributed with a distinctly even spacing between each vacancy layer. Consequently, the superstructure reflections along the [111] c directions (marked with blue arrows) are getting less diffuse and higher order superstructure reflections can be observed. At 280 °C, the samples transform into the thermodynamically stable phase and the vacancies are highly ordered along a single set of (111) c planes. As described above, the stable phase, in comparison to I and II, exhibits a



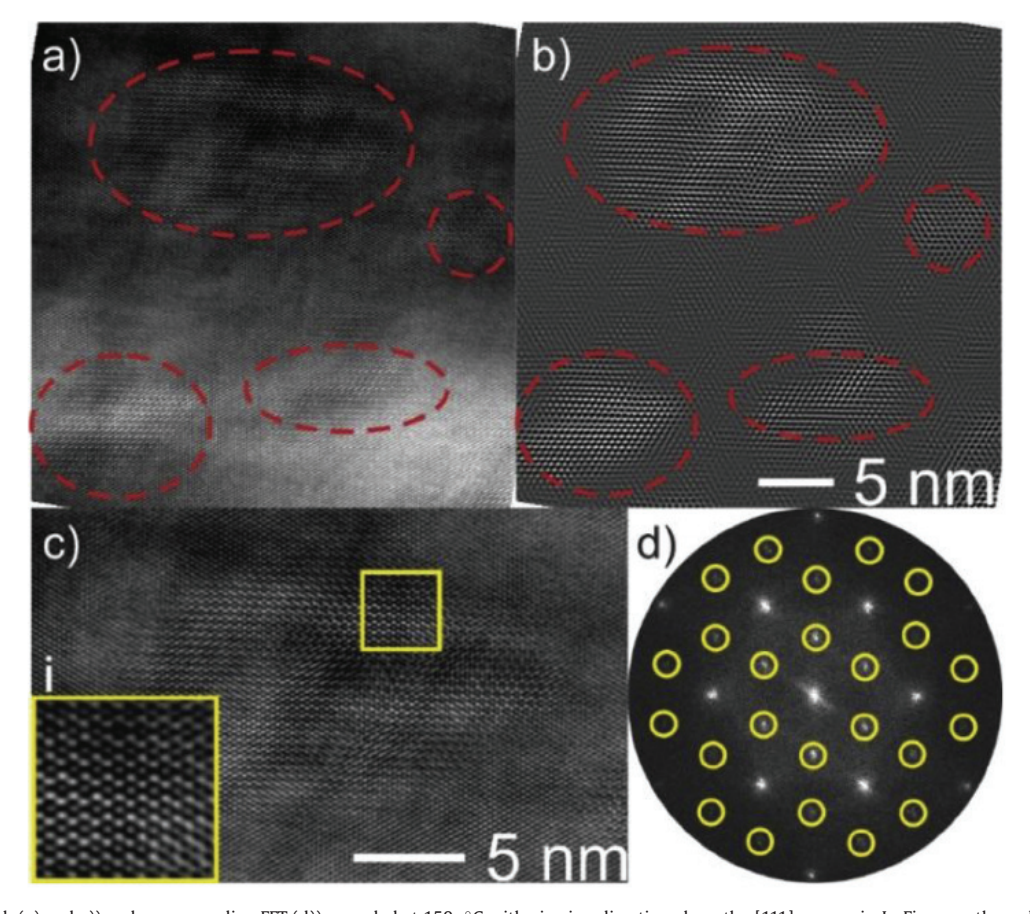
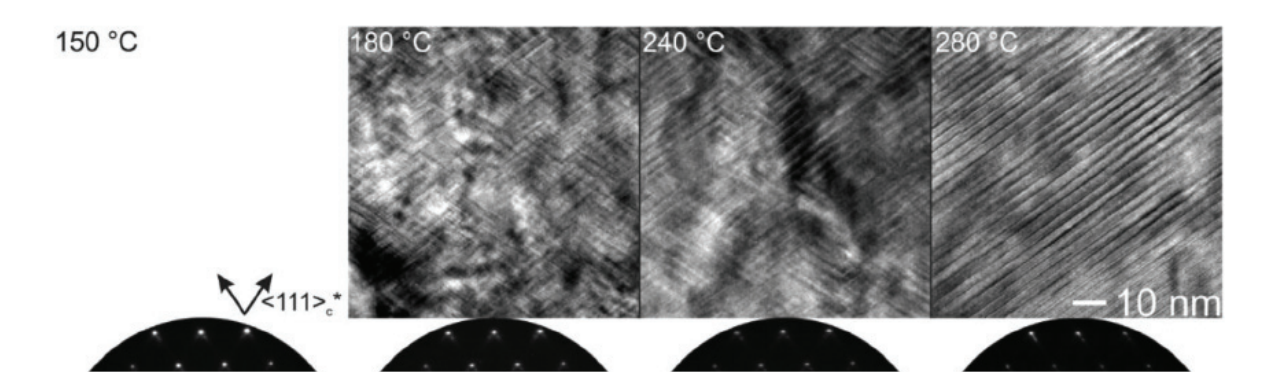


Fig. 5. HRTEM micrograph (a) and c)) and corresponding FFT (d)) recorded at 150 °C with viewing direction along the [111] zone axis. In Figure a, the red encircled regions mark domains formed during a phase transition due to ordering of vacancies. The inset of Figure c) represents an enlarged region of a domain showing a typical honeycomb arrangement of bright spots. The yellow circles in Figure d) highlight superstructure reflections used for inverse FFT filtering (Figure b)). The bright contrast in the upper right image highlights regions with significant contribution from the marked reflections. (For interpretation of the references to colour in this figure legend, the reader is referred to the Web version of this article.)



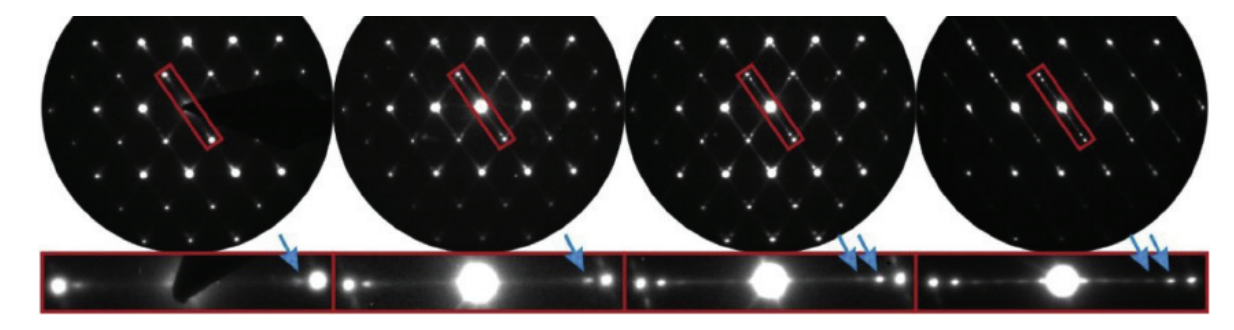


Fig. 6. Representative TEM micrographs (top) and electron diffraction patterns (bottom) taken at different temperatures. With increasing temperature, the ordering of the vacancies increases. At 280 °C, vacancies are highly ordered along one (111)c direction, and a transtition to the thermodynamically stable phase is observed. The enlarged sections of the regions marked in red hightlight the sharpening and increasing number of reflections as a result of increased vacancy ordering. Superstructure reflections are marked with blue arrows. (For interpretation of the references to colour in this figure legend, the reader is referred to the Web version of this article.)

C. Koch et al. / Acta Materialia 152 (2018) 278-287

284

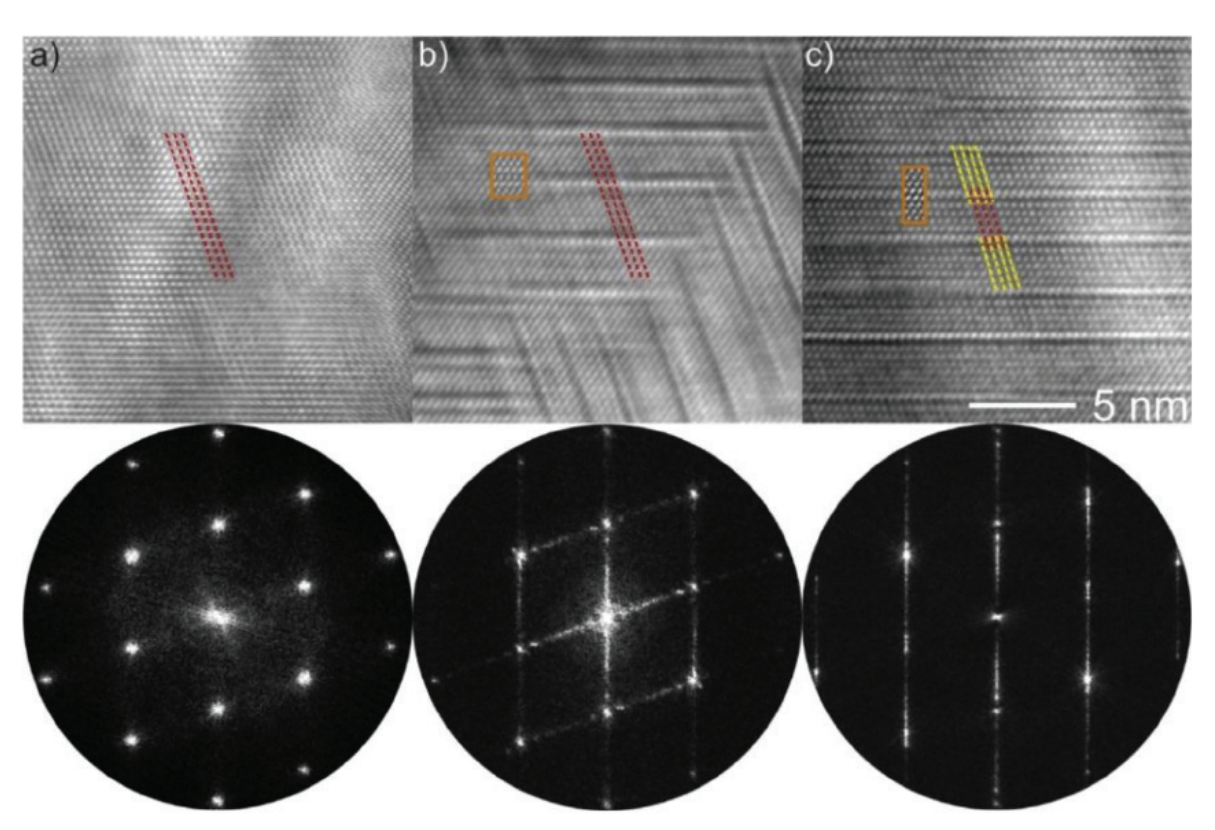


Fig. 7. HRTEM micrographs and corresponding FFTs of different Ge  $_6$ Sn $_2$ Sb $_2$ Te $_{11}$  structures. a) HRTEM micrograph of I with randomly distributed vacancies. The red dotted line highlights the cubic stacking sequence. b) Vacancies order inside the (111)c planes, forming vacancy layers and thus characteristic diffuse streaks in the FFT (II). Again, the red dotted line highlights the cubic like stacking sequence. Inset: TEM contrast simulation using a cell with similar stacking sequence as the one reported in Ref. [20] (defocus: 100 nm, thickness: 17.98 nm) c) Thermodynamically stable phase with van der Waals gaps. The stacking sequence across the van der Waals gaps is altered as indicated by yellow and red dotted lines. For HRTEM contrast simulations (inset), a cell with similar stacking sequence as reported in Refs. [9,77–79] was applied. (defocus: 14 nm, thickness: 11.47 nm). (For interpretation of the references to colour in this figure legend, the reader is referred to the Web version of this article.)

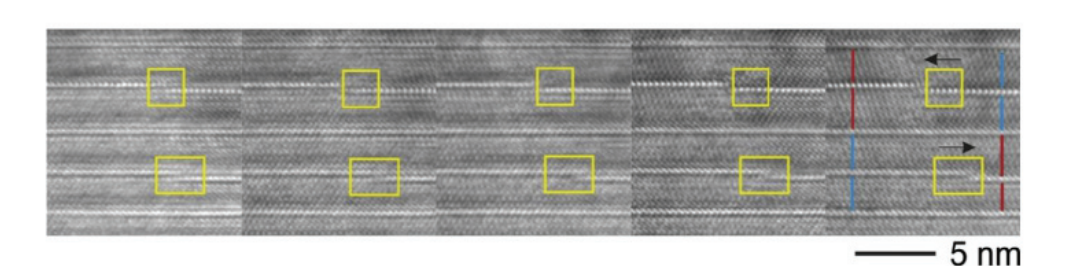


Fig. 8. HRTEM micrographs recorded sequentially (~4 s between each image) at 280 °C. The yellow rectangles mark so-called bilayer defects. Due to the temperature treatment,

stacking variance of Te-layers forming a van der Waals gap and can thus be distinguished by HRTEM micrographs in e.g. zone axis [110]<sub>c</sub> (see Fig. 7) [19,20].

Comparing the findings of Figs. 5 and 6, it can be seen that the observed contrast changes in the TEM micrographs and electron diffraction patterns in Fig. 6 are the result of a domain growth process. As shown in Fig. 5, the formation of domains is observed along [111] $_{\rm c}$  zone axis, tilting these domains by ~35°, which is approximately the tilting angle between (111) $_{\rm c}$  and (110) $_{\rm c}$ (cf. Fig. 4). This leads to overlapping of different domains and consequently to a superposition contrast including intersecting vacancy layers. This resembles the situation at 180 °C in Fig. 6 (center left). As the domains grow further and start to coalesce, domains with sizes of approximately the thickness of the film form and no superposition contrast is observed. These domains overlap only partly but are highly ordered with respect to the vacancy layer distance as

indicated by the contrast at 240  $^{\circ}$ C (cf. Fig. 6, center right). During the coalescence process, smaller domains vanish by forming larger domains which tend to be more stable, representing the transition observed between 240  $^{\circ}$ C and 300  $^{\circ}$ C.

Assuming that the coalescing domains exhibit a stacking disorder along the <111> direction (e.g. by different sizes of the distorted rock-salt like building blocks or simply by a stacking sequence mismatch), the diffuse streaks observed at 280 °C (Fig. 6, right) might reflect the lack of ordering at this stage. The HRTEM micrograph shown in Fig. 8 strengthens this interpretation, as a significant number of step-like defects are observed. In Fig. 8, rows of bright spots represent the van der Waals gaps between the distorted rock salt like building blocks. Bilayer defects [74], which appear as steps in the HRTEM micrographs (yellow rectangles in Fig. 8) separate regions with evenly and unevenly sized rock-salt type building blocks, which are highlighted by blue and red lines,

C. Koch et al. / Acta Materialia 152 (2018) 278-287



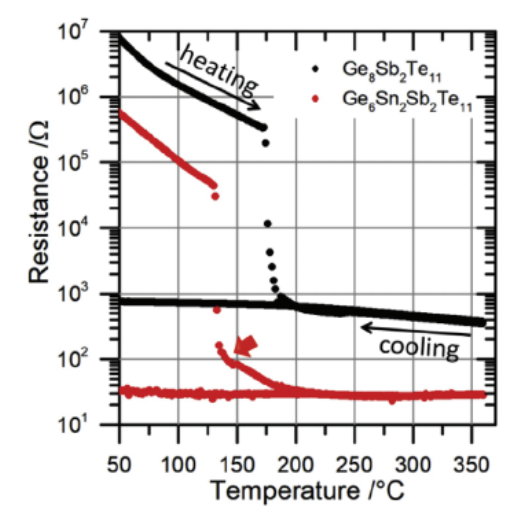


**Fig. 9.** Sheet resistance measurements of Ge  $_8$ Sb $_2$ Te $_{11}$  (black) and Ge  $_6$ Sn $_2$ Sb $_2$ Te $_{11}$  (red). The large drop of the resistance indicates the phase change temperatures. The continuous decrease after the first phase change in Ge  $_6$ Sn $_2$ Sb $_2$ Te $_{11}$  is the temperature region where the metastable phase I occurs. The small red arrow marks the possible extra step for multi-level data storage applications. (For interpretation of the references to colour in this figure legend, the reader is referred to the Web version of this article.)

respectively. After several seconds, the vacancies rearrange, thus reducing the sizes of the domains with unevenly sized building blocks (red lines) in favor of the domains with evenly sized building blocks (blue lines). Thus, the structure becomes increasingly ordered upon heating. This mechanism was recently proposed but could not be proven directly by means of *in situ* observation [80]. Here, the *in situ* observations allow a near atomistic look at the ordering process and the direct observation of the proposed mechanism for the first time. The atomistic processes accompanying the observed structural ordering still have to be determined, which provides a challenging question for future research [81,82].

## 3.2. Sheet resistance measurements

Results of the temperature dependent sheet resistance measurements are shown in Fig. 9. The sheet resistance of the amor-

contrast, the resistance of Ge  $_6$ Sn $_2$ Sb $_2$ Te $_{11}$  remains quite constant at 30 , suggesting that this compound is a small band gap semiconductor with pronounced disorder [83].

### 4. Conclusion and summary

In summary, our approach of combining *in situ* XRD and TEM observation along with physical property measurements gave new insights into the phase change mechanisms of tin substituted Ge<sub>8</sub>Sb<sub>2</sub>Te<sub>11</sub>. Ge<sub>6</sub>Sn<sub>2</sub>Sb<sub>2</sub>Te<sub>11</sub> shows an extra intermediate state between the amorphous and metastable crystalline phases, verified firstly by the combined approach of sheet resistance measurements and *in situ* TEM observations. It may be used in the switching process of electrical phase change memory devices as an additional distinguishable electrical state. As a result, tin substituted PCMs could be highly promising candidates for multi-level data storage applications.

## Acknowledgments

MW acknowledges support by the DFG (SFB 917). TD, DH and LK like to thank Lena Nolte and Igor Barg for their support in TEM data evaluation. Further, TD and DH acknowledge financial support by the federal state Schleswig-Holstein and the DFG (SPP 1386). LK acknowledges support by FOR 2093 and SFB 1261. DCJ acknowledges support from the National Science Foundation under grant DMR-1710214. Declaration of interest: none.

## Appendix A. Supplementary data

Supplementary data related to this article can be found at https://doi.org/10.1016/j.actamat.2018.04.029.

## References

- [1] S.R. Ovshinsky, Reversible electrical switching phenomena in disordered structures, Phys. Rev. Lett. 21 (1968) 1450.
- [2] M. Chen, K.A. Rubin, R.W. Barton, Compound materials for reversible, phase-change optical data storage, Appl. Phys. Lett. 49 (1986) 502, https://doi.org/10.1063/1.97617.
- [3] A.V. Kolobov, P. Fons, J. Tominaga, S.R. Ovshinsky, Vacancy-mediated threecenter four-electron bonds in GeTe-Sb <sub>2</sub>Te3 phase-change memory alloys, Phys. Rev. B 87 (2013), https://doi.org/10.1103/PhysRevB.87.165206.
- [4] N. Yamada, E. Ohno, K. Nishiuchi, N. Akahira, M. Takao, Rapid-phase transi-

phous phases at  $50\,^{\circ}$ C decreases from ~ $10\,M$  (Ge8Sb2Te11) to ~ $500\,k$  (Ge6Sn2Sb2Te11) which can be explained by the substitution of Ge by Sn resulting in a lower band gap. With increasing temperature, the resistance of the amorphous phase decreases slightly as expected for phase change materials. The actual phase change process is accompanied by a sudden drop of the resistance by 2.5 orders of magnitude at 174 °C for Ge<sub>8</sub>Sb<sub>2</sub>Te<sub>11</sub>. The phase change temperature determined here differs from those reported in the literature, which can be explained by different heating rates [51,56,57]. No change in resistivity due to the phase change in the thermodynamically stable phase was observed, demonstrating the similarity between the different crystalline phases with respect to their electrical properties. The sheet resistance behavior of Ge<sub>6</sub>Sn<sub>2</sub>Sb<sub>2</sub>Te<sub>11</sub>, on the other hand, differs from that of the unsubstituted material in a unique way. Immediately following the abrupt drop of two orders of magnitude in electrical resistance at 132 °C there is a continuous second reduction of the resistance. The different electrical behaviors might be the result of the presence of I and II, both crystallizing far below the phase change temperature to the thermodynamically stable phase. This finding is in good agreement with the results of the TEM investigations.

The resistance of the stable phase of Ge <sub>8</sub>Sb<sub>2</sub>Te<sub>11</sub> increases with decreasing temperature revealing semi-conducting behavior. In

- tions of GeTe-Sb <sup>2</sup>Te<sup>3</sup> pseudobinary amorphous thin films for an optical disk memory, J. Appl. Phys. 69 (1991) 2849, https://doi.org/10.1063/1.348620. H.-Y. Cheng, S. Raoux, J.L. Jordan-Sweet, Crystallization properties of materials
- [5] H.-Y. Cheng, S. Raoux, J.L. Jordan-Sweet, Crystallization properties of materials along the pseudo-binary line between GeTe and Sb, J. Appl. Phys. 115 (2014) 093101, https://doi.org/10.1063/1.4867045.
- [6] J. Akola, R.O. Jones, Structure of amorphous Ge 8Sb<sub>2</sub>Te<sub>11</sub>: GeTe-Sb<sub>2</sub>Te<sub>3</sub> alloys and optical storage, Phys. Rev. B 79 (2009), https://doi.org/10.1103/ PhysRevB.79.134118.
- [7] N. Yamada, E. Ohno, N. Akahira, K. Nishiuchi, K. Nagata, M. Takao, High speed overwritable phase change optical disk material, Jpn. J. Appl. Phys. 26 (1987) 61–66
- [8] T. Matsunaga, R. Kojima, N. Yamada, K. Kifune, Y. Kubota, Y. Tabata, M. Takata, Single structure widely distributed in a GeTe—Sb <sub>2</sub>Te<sub>3</sub> pseudobinary system: a rock salt structure is retained by intrinsically containing an enormous number of vacancies within its crystal, lnorg. Chem. 45 (2006) 2235—2241, https:// doi.org/10.1021/ic051677w.
- [9] T. Matsunaga, H. Morita, R. Kojima, N. Yamada, K. Kifune, Y. Kubota, Y. Tabata, J.-J. Kim, M. Kobata, E. Ikenaga, K. Kobayashi, Structural characteristics of GeTe-rich GeTe-Sb<sub>2</sub>Te<sub>3</sub> pseudobinary metastable crystals, J. Appl. Phys. 103 (2008) 093511, https://doi.org/10.1063/1.2901187.
- [10] M. Wuttig, N. Yamada, Phase-change materials for rewriteable data storage, Nat. Mater. 6 (2007) 824–832.
- [11] M. Krbal, A.V. Kolobov, P. Fons, J. Tominaga, S.R. Elliott, J. Hegedus, T. Uruga, Intrinsic complexity of the melt-quenched amorphous Ge 2Sb2Te5 memory alloy, Phys. Rev. B 83 (2011), https://doi.org/10.1103/PhysRevB.83.054203.
- [12] C. Lang, S. Song, D. Manh, D. Cockayne, Building blocks of amorphous Ge<sub>2</sub>Sb<sub>2</sub>Te<sub>5</sub>, Phys. Rev. B 76 (2007), https://doi.org/10.1103/ PhysRevB.76.054101.
- [13] J. Da Silva, A. Walsh, H. Lee, Insights into the structure of the stable and metastable (GeTe)m(Sb<sub>2</sub>Te<sub>3</sub>)n compounds, Phys. Rev. B 78 (2008), https://

#### C. Koch et al. / Acta Materialia 152 (2018) 278-287

#### doi.org/10.1103/PhysRevB.78.224111.

286

- [14] T.H. Lee, S.R. Elliott, Structural role of vacancies in the phase transition of Ge<sub>2</sub>Sb<sub>2</sub>Te<sub>5</sub> memory materials, Phys. Rev. B 84 (2011), https://doi.org/10.1103/ PhysRevB 84 094124
- [15] J. Zhou, Z. Sun, Y. Pan, Z. Song, R. Ahuja, Vacancy or not: an insight on the intrinsic vacancies in rocksalt-structured GeSbTe alloys from ab initio calculations, EPL Europhys. Lett. 95 (2011) 27002, https://doi.org/10.1209/0295-5075/95/27002.
- [16] S. Kohara, K. Kato, S. Kimura, H. Tanaka, T. Usuki, K. Suzuya, H. Tanaka, Y. Moritomo, T. Matsunaga, N. Yamada, Y. Tanaka, H. Suematsu, M. Takata, Structural basis for the fast phase change of Ge <sub>2</sub>Sb<sub>2</sub>Te<sub>5</sub>: ring statistics analogy between the crystal and amorphous states, Appl. Phys. Lett. 89 (2006) 201910, https://doi.org/10.1063/1.2387870.
- [17] J. Akola, R. Jones, Structural phase transitions on the nanoscale: the crucial pattern in the phase-change materials Ge 2Sb2Te5 and GeTe, Phys. Rev. B 76 (2007). https://doi.org/10.1103/PhysRevB.76.235201.
- (2007), https://doi.org/10.1103/PhysRevB.76.235201.
   [18] U. Ross, A. Lotnyk, E. Thelander, B. Rauschenbach, Direct imaging of crystal structure and defects in metastable Ge 2Sb<sub>2</sub>Te<sub>5</sub> by quantitative aberration-corrected scanning transmission electron microscopy, Appl. Phys. Lett. 104 (2014) 121904, https://doi.org/10.1063/1.4869471.
- [19] B. Zhang, X.-P. Wang, Z.-J. Shen, X.-B. Li, C.-S. Wang, Y.-J. Chen, J.-X. Li, J.-X. Zhang, Z. Zhang, S.-B. Zhang, X.-D. Han, Vacancy structures and melting behavior in rock-salt GeSbTe, Sci. Rep. 6 (2016), https://doi.org/10.1038/srep25453.
- [20] T. Rosenthal, S. Welzmiller, L. Neudert, P. Urban, A. Fitch, O. Oeckler, Novel superstructure of the rocksalt type and element distribution in germanium tin antimony tellurides, J. Solid State Chem. 219 (2014) 108–117, https://doi.org/ 10.1016/j.jssc.2014.07.014.
- [21] D. Lencer, M. Salinga, M. Wuttig, Design rules for phase-change materials in data storage applications, Adv. Mater. 23 (2011) 2030–2058, https://doi.org/ 10.1002/adma.201004255.
- [22] R. Waser, R. Dittmann, M. Salinga, M. Wuttig, Function by defects at the atomic scale – new concepts for non-volatile memories, Solid State Electron. 54 (2010) 830–840, https://doi.org/10.1016/j.sse.2010.04.043.
- [23] T. Nirschl, J.B. Philipp, T.D. Happ, G.W. Burr, B. Rajendran, M.-H. Lee, A. Schrott, M. Yang, M. Breitwisch, C.-F. Chen, others, Write strategies for 2 and 4-bit multi-level phase-change memory, in: Electron Devices Meet. 2007 IEDM 2007 IEEE Int, IEEE, 2007, pp. 461–464.
- [24] S. Raoux, D. Ielmini, M. Wuttig, I. Karpov, Phase change materials, MRS Bull. 37 (2012) 118–123.
- [25] S. Raoux, H.-Y. Cheng, M.A. Caldwell, H.-S.P. Wong, Crystallization times of Ge—Te phase change materials as a function of composition, Appl. Phys. Lett. 95 (2009) 071910, https://doi.org/10.1063/1.3212732.
- [26] D. Baker, M. Paesler, G. Lucovsky, S. Agarwal, P. Taylor, Application of bond constraint theory to the switchable optical memory material Ge 2Sb<sub>2</sub>Te<sub>5</sub>, Phys. Rev. Lett. 96 (2006), https://doi.org/10.1103/PhysRevLett.96.255501.
- [27] W.P. Zhou, F.R. Liu, N. Bai, Y.H. Wan, X. Lin, J.M. Chen, Crystallization of amorphous Ge<sub>2</sub>Sb<sub>2</sub>Te<sub>5</sub>films induced by an ultraviolet laser, Appl. Surf. Sci. 285 (2013) 97–101, https://doi.org/10.1016/j.apsusc.2013.07.082.
- [28] B.-S. Lee, R.M. Shelby, S. Raoux, C.T. Retter, G.W. Burr, S.N. Bogle, K. Darmawikarta, S.G. Bishop, J.R. Abelson, Nanoscale nuclei in phase change

#### 10.1063/1.4842175.

- [39] T.G. Edwards, I. Hung, Z. Gan, B. Kalkan, S. Raoux, S. Sen, Structural transformations in amorphous crystalline phase change of Ga-Sb alloys, J. Appl. Phys. 114 (2013) 233512, https://doi.org/10.1063/1.4854575.
- [40] Y. Saito, Y. Sutou, J. Koike, Optical contrast and laser-induced phase transition in GeCu<sub>2</sub>Te<sub>3</sub> thin film, Appl. Phys. Lett. 102 (2013) 051910, https://doi.org/ 10.1063/1.4791567
- [41] S. Shindo, Y. Sutou, J. Koike, Y. Saito, Y.-H. Song, Contact resistivity of amorphous and crystalline GeCu<sub>2</sub>Te<sub>3</sub> to W electrode for phase change random access memory, Mater. Sci. Semicond. Process. 47 (2016) 1–6, https://doi.org/10.1016/j.mssp.2016.02.006.
- [42] K. Kamimura, K. Kimura, S. Hosokawa, N. Happo, H. Ikemoto, Y. Sutou, S. Shindo, Y. Saito, J. Koike, XAFS analysis of crystal GeCu <sub>2</sub>Te<sub>3</sub> phase change material, Z. Phys. Chem. 230 (2016), https://doi.org/10.1515/zpch-2015-0672.
- [43] M. Salinga, E. Carria, A. Kaldenbach, M. Bornh offt, J. Benke, J. Mayer, M. Wuttig, Measurement of crystal growth velocity in a melt-quenched phase-change material, Nat. Commun. 4 (2013), https://doi.org/10.1038/ncomms3371.
- [44] C.N. Afonso, J. Solis, F. Catalina, C. Kalpouzos, Ultrafast reversible phase change in GeSb films for erasable optical storage, Appl. Phys. Lett. 60 (1992) 3123, https://doi.org/10.1063/1.106772.
- [45] P. Zalden, C. Bichara, J. van Eijk, C. Braun, W. Bensch, M. Wuttig, Atomic structure of amorphous and crystallized Ge <sub>15</sub>Sb <sub>85</sub>, J. Appl. Phys. 107 (2010) 104312, https://doi.org/10.1063/1.3380667.
- [46] M. Putero, M.-V. Coulet, C. Muller, C. Baehtz, S. Raoux, H.-Y. Cheng, Ge-doped GaSb thin films with zero mass density change upon crystallization for applications in phase change memories, Appl. Phys. Lett. 108 (2016) 101909, https://doi.org/10.1063/1.4943788.
- [47] R.M. Shelby, S. Raoux, Crystallization dynamics of nitrogen-doped Ge <sub>2</sub>Sb<sub>2</sub>Te<sub>5</sub>, J. Appl. Phys. 105 (2009) 104902, https://doi.org/10.1063/1.3126501.
- [48] B. Liu, Z. Song, T. Zhang, J. Xia, S. Feng, B. Chen, Effect of N-implantation on the structural and electrical characteristics of Ge <sub>2</sub>Sb<sub>2</sub>Te<sub>5</sub> phase change film, Thin Solid Films 478 (2005) 49–55, https://doi.org/10.1016/j.tsf.2004.09.057.
- [49] X. Zhou, L. Wu, Z. Song, F. Rao, M. Zhu, C. Peng, D. Yao, S. Song, B. Liu, S. Feng, Carbon-doped Ge<sub>2</sub>Sb<sub>2</sub>Te<sub>5</sub> phase change material: a candidate for high-density phase change memory application, Appl. Phys. Lett. 101 (2012) 142104, https://doi.org/10.1063/1.4757137.
- [50] K. Wang, C. Steimer, D. Wamwangi, S. Ziegler, M. Wuttig, Effect of indium doping on Ge 2Sb2Te5 thin films for phase-change optical storage, Appl. Phys. A 80 (2005) 1611–1616, https://doi.org/10.1007/s00339-005-3232-2.
- [51] C. Koch, A.-L. Hansen, T. Dankwort, G. Schienke, M. Paulsen, D. Meyer, M. Wimmer, M. Wuttig, L. Kienle, W. Bensch, Enhanced temperature stability and exceptionally high electrical contrast of selenium substituted Ge <sub>2</sub>Sb<sub>2</sub>Te<sub>5</sub> phase change materials, RSC Adv. 7 (2017) 17164–17172, https://doi.org/ 10.1039/C7RA01140G.
- [52] K. Wang, C. Steimer, D. Wamwangi, S. Ziegler, M. Wuttig, J. Tomforde, W. Bensch, Influence of doping upon the phase change characteristics of Ge<sub>2</sub>Sb<sub>2</sub>Te<sub>5</sub>, Microsyst. Technol. 13 (2006) 203–206, https://doi.org/10.1007/ s00542-006-0156-5.
- [53] E.M. Vinod, K. Ramesh, K.S. Sangunni, Structural transition and enhanced phase transition properties of Se doped Ge<sub>2</sub>Sb<sub>2</sub>Te<sub>5</sub> alloys, Sci. Rep. 5 (2015) 8050, https://doi.org/10.1038/srep08050.

- [29] P. Rodenbach, A. Giussani, K. Perumal, M. Hanke, M. Dubslaff, H. Riechert, R. Calarco, M. Burghammer, A.V. Kolobov, P. Fons, Recrystallization of an amorphized epitaxial phase-change alloy: a phoenix arising from the ashes, Appl. Phys. Lett. 101 (2012) 061903, https://doi.org/10.1063/1.4742919.
- [30] N. Yamada, T. Matsunaga, Structure of laser-crystallized Ge <sub>2</sub>Sb<sub>2</sub>Te<sub>5</sub> sputtered thin films for use in optical memory, J. Appl. Phys. 88 (2000) 7020, https:// doi.org/10.1063/1.1314323.
- [31] I. Friedrich, V. Weidenhof, W. Njoroge, P. Franz, M. Wuttig, Structural transformations of Ge<sub>2</sub>Sb<sub>2</sub>Te<sub>5</sub> films studied by electrical resistance measurements, J. Appl. Phys. 87 (2000) 4130, https://doi.org/10.1063/1.373041.
- [32] V. Weidenhof, I. Friedrich, S. Ziegler, M. Wuttig, Laser induced crystallization of amorphous Ge<sub>2</sub>Sb<sub>2</sub>Te<sub>5</sub> films, J. Appl. Phys. 89 (2001) 3168, https://doi.org/ 10.1063/1.1351868.
- [33] G.-F. Zhou, Materials aspects in phase change optical recording, Mater. Sci. Eng. A 304 (2001) 73–80, https://doi.org/10.1016/S0921-5093(00)01448-9.
- [34] B.J. Kooi, W.M.G. Groot, J.T.M. De Hosson, In situ transmission electron microscopy study of the crystallization of Ge <sub>2</sub>Sb<sub>2</sub>Te<sub>5</sub>, J. Appl. Phys. 95 (2004) 924–932, https://doi.org/10.1063/1.1636259.
- [35] G. Ruitenberg, A.K. Petford-Long, R.C. Doole, Determination of the isothermal nucleation and growth parameters for the crystallization of thin Ge <sub>2</sub>Sb<sub>2</sub>Te<sub>5</sub> films, J. Appl. Phys. 92 (2002) 3116–3123, https://doi.org/10.1063/1.1503166.
- [36] M. Krbal, A.V. Kolobov, P. Fons, R.E. Simpson, T. Matsunaga, J. Tominaga, N. Yamada, Local atomic order of crystalline Ge <sub>8</sub>Sb<sub>2</sub>Te<sub>11</sub> across the ferroelectric to paraelectric transition: the role of vacancies and static disorder, Phys. Rev. B 84 (2011), https://doi.org/10.1103/PhysRevB.84.104106.
- [37] M. Putero, M.-V. Coulet, T. Ouled-Khachroum, C. Muller, C. Baehtz, S. Raoux, Unusual crystallization behavior in Ga-Sb phase change alloys, Apl. Mater. 1 (2013) 062101, https://doi.org/10.1063/1.4833035.
- [38] M. Putero, M.-V. Coulet, T. Ouled-Khachroum, C. Muller, C. Baehtz, S. Raoux, Phase transition in stoichiometric GaSb thin films: anomalous density change and phase segregation, Appl. Phys. Lett. 103 (2013) 231912, https://doi.org/

- [54] E.M. Vinod, K. Ramesh, R. Ganesan, K.S. Sangunni, Direct hexagonal transition of amorphous (Ge2Sb2Te5)0.9Se0.1 thin films, Appl. Phys. Lett. 104 (2014) 063505, https://doi.org/10.1063/1.4865198.
- [55] R. Svoboda, V. Karabyn, J. M alek, M. Frumar, L. Benes, M. Vlček, Amorphous-to-crystalline transition in Ge <sub>8</sub>Sb<sub>(2-x)</sub>Bi<sub>x</sub>Te<sub>11</sub> phase-change materials for data recording, J. Alloy. Comp. 674 (2016) 63–72, https://doi.org/10.1016/j.jallcom.2016.03.019.
- [56] C. Koch, G. Schienke, M. Paulsen, D. Meyer, M. Wimmer, H. Volker, M. Wuttig, W. Bensch, Investigating the influence of resonant bonding on the optical properties of phase change materials (GeTe) xSnSb<sub>2</sub>Se<sub>4</sub>, Chem. Mater. 29 (2017) 9320–9327, https://doi.org/10.1021/acs.chemmater.7b03299.
- [57] S. Buller, C. Koch, W. Bensch, P. Zalden, R. Sittner, S. Kremers, M. Wuttig, U. Schürmann, L. Kienle, T. Leichtweiß, J. Janek, B. Schönborn, Influence of partial substitution of Te by Se and Ge by Sn on the properties of the blu-ray phase-change material Ge<sub>8</sub>Sb<sub>2</sub>Te<sub>11</sub>, Chem. Mater. 24 (2012) 3582–3590, https://doi.org/10.1021/cm301809g.
- [58] T. Rosenthal, M.N. Schneider, C. Stiewe, M. D öblinger, O. Oeckler, Real structure and thermoelectric properties of GeTe-rich germanium antimony tellurides, Chem. Mater. 23 (2011) 4349–4356, https://doi.org/10.1021/cm201717z.
- [59] M.N. Schneider, T. Rosenthal, C. Stiewe, O. Oeckler, From phase-change materials to thermoelectrics? Z. Kristallogr. 225 (2010) https://doi.org/10.1524/zkri.2010.1320.
- [60] T. Rosenthal, P. Urban, K. Nimmrich, L. Schenk, J. de Boor, C. Stiewe, O. Oeckler, Enhancing the thermoelectric properties of germanium antimony tellurides by substitution with selenium in compounds Ge  $_n$ Sb<sub>2</sub> (Te<sub>1-x</sub>Se<sub>x</sub>) $_n+3$ (0  $\leq x \leq$  0.5;  $n \geq 7$ ), Chem. Mater. 26 (2014) 2567–2578, https://doi.org/10.1021/cm404115k.
- [61] F. Fahrnbauer, D. Souchay, G. Wagner, O. Oeckler, High thermoelectric figure of merit values of germanium antimony tellurides with kinetically stable cobalt germanide precipitates, J. Am. Chem. Soc. 137 (2015) 12633–12638, https://doi.org/10.1021/jacs.5b07856.
- [62] N. Bai, F.R. Liu, X.X. Han, Z. Zhu, F. Liu, X. Lin, N.X. Sun, A study on the crystallization behavior of Sn-doped amorphous Ge <sub>2</sub>Sb<sub>2</sub>Te<sub>5</sub> by ultraviolet laser

C. Koch et al. / Acta Materialia 152 (2018) 278-287

287

- radiation, Appl. Surf. Sci. 316 (2014) 202–206, https://doi.org/10.1016/j.apsusc.2014.08.007.
- [63] N. Bai, F. Liu, X. Han, Z. Zhu, F. Liu, X. Lin, N.X. Sun, Effect of the Sn dopant on the crystallization of amorphous Ge<sub>2</sub>Sb<sub>2</sub>Te<sub>5</sub> films induced by an excimer laser, Optic Laser. Technol. 74 (2015) 11–15, https://doi.org/10.1016/ j.optlastec.2015.03.019.
- [64] G. Singh, A. Kaura, M. Mukul, S.K. Tripathi, Electrical, optical, and thermal properties of Sn-doped phase change material Ge 25b2Te5, J. Mater. Sci. 48 (2013) 299–303, https://doi.org/10.1007/s10853-012-6745-z.
- [65] A.A. Coelho, Topas-academic, Coelho Software, Brisbane, Australia, 2016.
- [66] R.W. Cheary, A. Coelho, A fundamental parameters approach to X-ray line-profile fitting, J. Appl. Crystallogr. 25 (1992) 109–121.
- [67] D.R.G. Mitchell, B. Schaffer, Scripting-customised microscopy tools for digital Micrograph™, Ultramicroscopy 103 (2005) 319–332, https://doi.org/10.1016/ i.ultramic.2005.02.003.
- [68] M. Wimmer, M. Kaes, C. Dellen, M. Salinga, Role of activation energy in resistance drift of amorphous phase change materials, Front. Physiol. 2 (2014), https://doi.org/10.3389/fphy.2014.00075.
- [69] L.J. van der Pauw, A method of measuring specific resistivity and Hall effect of discs of arbitrary shape, Philips Res. Rep. 13 (1958) 1–9.
- [70] L.J. van der Pauw, A method of measuring the resistivity and Hall coefficient on lamellae of arbitrary shape, Philips Res. Rep. 20 (1958) 220–224.
- [71] I.E. Bolotov, V.Y. Kolosov, A.V. Kozhyn, Electron microscope investigation of crystals based on bend-contour arrangement II. Bending phenomena of the crystal growth in an amorphous film, Phys. Status Solidi 72 (1982) 645–654, https://doi.org/10.1002/pssa.2210720226.
- [72] A. Lotnyk, S. Bernütz, X. Sun, U. Ross, M. Ehrhardt, B. Rauschenbach, Real-space imaging of atomic arrangement and vacancy layers ordering in laser crystallised Ge<sub>2</sub>Sb<sub>2</sub>Te<sub>5</sub> phase change thin films, Acta Mater. 105 (2016) 1–8, https://doi.org/10.1016/j.actamat.2015.12.010.
- [73] L. Kienle, M. Schlosser, M.J. Manos, C.D. Malliakas, V. Duppel, C. Reiner, H.-J. Deiseroth, M.G. Kanatzidis, K. Kelm, A. Simon, Ordering phenomena in complex chalcogenides – the showcase of A<sub>2</sub>In<sub>12</sub>Q<sub>19</sub> (a = K, Tl, NH<sub>4</sub>; Q = Se, Te) and pseudobinary In<sub>2</sub>Q<sub>3</sub>, Eur. J. Inorg. Chem. 2010 (2010) 367–378,

- https://doi.org/10.1002/ejic.200900721.
- [74] A. Lotnyk, U. Ross, T. Dankwort, I. Hilmi, L. Kienle, B. Rauschenbach, Atomic structure and dynamic reconfiguration of layered defects in van der Waals layered Ge-Sb-Te based materials, Acta Mater. 141 (2017) 92–96, https://doi.org/10.1016/j.actamat.2017.09.012.
- [75] L. Kienle, O. Oeckler, H. Mattausch, V. Duppel, A. Simon, C. Reiner, M. Schlosser, K. Xhaxhiu, H.J. Deiseroth, Real structure of partially ordered crystals, Mater. Sci. Semicond. Process. 6 (2003) 393–396, https://doi.org/ 10.1016/j.mssp.2003.07.009.
- [76] L. Kienle, V. Duppel, A. Simon, H.J. Deiseroth, Realstrukturen von Defektvarianten des Zinkblendetyps, Z. Für Anorg, Allg. Chem. 629 (2003) 1412–1420, https://doi.org/10.1002/zaac.200300113.
- [77] L.E. Shelimova, O.G. Karpinskii, V.S. Zemskov, P.P. Konstantinov, Structural and electrical properties of layered tetradymite-like compounds in the GeTe—Bi <sub>2</sub>Te<sub>3</sub> and GeTe—Sb<sub>2</sub>Te<sub>3</sub> systems, Inorg. Mater. 36 (2000) 235–242, https://doi.org/10.1007/BF02757928.
- [78] U. Schürmann, V. Duppel, S. Buller, W. Bensch, L. Kienle, Precession electron diffraction - a versatile tool for the characterization of phase change materials, Cryst. Res. Technol. 46 (2011) 561–568, https://doi.org/10.1002/ crat.201000516.
- [79] D.L. Medlin, G.J. Snyder, Atomic-Scale interfacial structure in rock salt and tetradymite chalcogenide thermoelectric materials, JOM (J. Occup. Med.) 65 (2013) 390–400, https://doi.org/10.1007/s11837-012-0530-y.
- [80] J. Momand, R. Wang, J.E. Boschker, M.A. Verheijen, R. Calarco, B.J. Kooi, Dynamic reconfiguration of van der Waals gaps within GeTe–Sb 2Te<sub>3</sub> based superlattices, Nanoscale (2017), https://doi.org/10.1039/C7NR01684K.
- [81] X. Yu, J. Robertson, Modeling of switching mechanism in GeSbTe chalcogenide superlattices, Sci. Rep. 5 (2015), https://doi.org/10.1038/srep12612.
- [82] X. Yu, J. Robertson, Atomic layering, intermixing and switching mechanism in Ge-Sb-Te based chalcogenide superlattices, Sci. Rep. 6 (2016), https://doi.org/ 10.1038/srep37325.
- [83] T. Siegrist, P. Jost, H. Volker, M. Woda, P. Merkelbach, C. Schlockermann, M. Wuttig, Disorder-induced localization in crystalline phase-change materials, Nat. Mater. 10 (2011) 202–208, https://doi.org/10.1038/nmat2934.